UIOWA-94-10

Hadron collider limits on anomalous $WW\gamma$ couplings

Kevin R. Barger and M. H. Reno

Department of Physics and Astronomy,

University of Iowa, Iowa City, IA 52242, USA

A next-to-leading log calculation of the reactions pp and $p\overline{p} \to W^{\pm}\gamma X$ is presented including a tri-boson gauge coupling from non-Standard Model contributions. The additional term arises by considering the Standard Model as a low energy effective theory. Two approaches are made for comparison. The first approach considers the tri-boson $WW\gamma$ coupling as being uniquely fixed by tree level unitarity at high energies to its Standard Model form and, consequently, suppresses the non-Standard Model contributions with form factors. The second approach is to ignore such considerations and calculate the contributions to non-Standard Model tri-boson gauge couplings without such suppressions, the idea being that at sufficiently high energies where new physics occurs, one abandons the low energy effective theory. It is found that at Tevatron energies, the two approaches do not differ much in quantitative results, while at Large Hadron Collider (LHC) energies the two approaches give significantly different predictions for production rates. At the Tevatron and LHC, however, the sensitivity limits on the anomalous coupling of $WW\gamma$ are too weak to usefully constrain parameters in effective Lagrangian models.

I. INTRODUCTION

With the advent of hadron supercolliders, it will be possible to directly test the tri-boson couplings of the W, Z and photon. Indeed, observations of the $WW\gamma$ coupling have been reported from measurements of $\sigma(p\overline{p} \rightarrow W^{\pm}\gamma)$ [1–3]. Experimental measurements coupled with accurate theoretical predictions could result in the confirmation of the Standard Model (SM), or alternatively, could point to new physics above the Z mass scale. The tri-boson couplings are uniquely constrained in the Standard Model if the gauge symmetry is $\mathrm{SU}(2) \otimes \mathrm{U}(1)$, the symmetry breaking sector is given by a minimally coupled, scalar Higgs boson, and the theory is renormalizable. If the Higgs boson as described by the SM is not the final word, the possibility exists that the SM is a low energy approximation to a more fundamental theory. In this case, non-Standard Model (NSM) effects may modify the tri-boson couplings.

The specific process $p\bar{p}$ or pp production of $W^{\pm}\gamma$ is of particular interest, in part because of the presence of an amplitude zero. In the parton center of mass frame, a zero in the amplitude occurs at a fixed angle between the quark and photon momenta [4,5]. In moving from the parton center of mass frame to the hadron collider frame, the zero translates to a dip in the angular distribution of the photon. Anomalous $WW\gamma$ couplings result in contributions that fill in the zero, making the $W^{\pm}\gamma$ production process especially sensitive to nonstandard effects at leading order. This has been explored in the literature by a variety of authors [6–9]. Some of these authors treat the anomalous $WW\gamma$ couplings as constants [6] while others include form factors multiplying the NSM parameters [7–9].

It has also been shown that strong interaction corrections [10–15] fill in the dip in the photon angular distribution. Thus, the strong interaction corrections must be well understood before one can claim evidence of new physics. The next-to-leading order calculation of $W\gamma$ production, including non-standard couplings, has been performed by Baur, Han and Ohnemus in Ref. [14]. However, their estimation of the sensitivities of the Fermilab Tevatron and supercolliders to nonstandard couplings was done using form factors. In the effective

Lagrangian approach of Ref. [6], however, there are no form factors multiplying the NSM parameters, but neither are strong interaction corrections included. At leading order and next-to-leading order in QCD, the two approaches to incorporating nonstandard couplings (with and without form factor suppression) lead to significant differences in $W^{\pm}\gamma$ production rates for the Large Hadron Collider (LHC). The focus of this paper is the comparison of the two approaches, including the $O(\alpha_s)$ corrections, to $W^{\pm}\gamma$ production at the Tevatron and LHC.

The rest of this paper is organized as follows: In Section II, brief descriptions of non-standard couplings and the Monte Carlo method incorporating the QCD corrections are included. Experimental cuts and approximations of the method are described along with some of the theoretical uncertainties. In Section III, the results are presented. Conclusions are presented in Section IV.

II. CALCULATION

A. Non-Standard Couplings

The calculations of Baur, Han and Ohnemus in Ref. [14] are based on a phenomenological Lagrangian,

$$\mathcal{L}_{WW\gamma} = -\mathrm{i}e\Big(W^{\dagger}_{\mu\nu}W^{\mu}A^{\nu} - W^{\dagger}_{\mu}A_{\nu}W^{\mu\nu} + \kappa W^{\dagger}_{\mu}W_{\nu}F^{\mu\nu} + \frac{\lambda}{M_W^2}W^{\dagger}_{\lambda\mu}W^{\mu}_{\nu}F^{\nu\lambda}\Big) \tag{1}$$

where A^{μ} and W^{μ} are the photon and W fields, respectively. The field strength tensors have the usual definitions for Abelian and non-Abelian gauge fields. In the standard model, $\kappa = 1$ and is related to the W magnetic dipole moment μ and electric quadrupole moment Q by

$$\mu = (1+\kappa)\frac{e}{2M_W}, \quad Q = -\kappa\frac{2e}{M_W^2}. \tag{2}$$

The standard model value for λ is $\lambda = 0$. In Ref. [14] , the NSM calculation is performed with $\Delta\kappa = \kappa - 1$ and λ of Eq. (1) scaling as

$$\Delta\kappa(M^2_{W\gamma}, p^2_W = M^2_W, p^2_\gamma = 0) = \frac{\Delta\kappa_0}{(1 + M^2_{W\gamma}/\Lambda^2)^n}. \tag{3}$$

$$\lambda(M^2_{W\gamma}, p^2_W = M^2_W, p^2_\gamma = 0) = \frac{\lambda_0}{(1 + M^2_{W\gamma}/\Lambda^2)^n}, \tag{4}$$

to preserve unitarity at asymptotically high energies. Here Λ is the scale at which new physics becomes important, $M^2_{W\gamma}$ is the invariant mass of the $W\gamma$ system, and λ_0 and κ_0 are the coupling parameters at low energy appearing in Eq. (1). In what follows, we drop the subscripts on κ and λ, and we indicate explicitly when the form factor is included.

Presumably $\Lambda \gg M_Z$ where M_Z is the Z mass. In the calculation presented here, Λ is taken as 1 TeV and $n = 2$ in the form factors, as in Ref. [14]. These form factors correspond to dipole factors similar to the roles played by the nucleon electric and magnetic dipole form factors appearing in deep inelastic scattering experiments. In those experiments [16], it is found empirically that the nucleon form factors have an approximate dipole form at low energies. There is, however, no *a priori* reason to expect the same here.

Longhitano has demonstrated in Ref. [17] that the most general CP conserving, dimension four operators which preserves the $\mathrm{SU}(2) \otimes \mathrm{U}(1)$ symmetry in the effective Lagrangian approach for the $WW\gamma$ vertex leads to the standard model terms, plus a term with $\Delta\kappa \neq 0$. In what follows, the parameter λ of Eq. (1) is ignored and the only NSM parameter of concern is $\Delta\kappa$. The notation of Ref. [6] has $\Delta\kappa$ is written in terms of the parameter $\hat{x}$:

$$\Delta\kappa = \frac{e^2\hat{x}}{16\pi^2 s^2_Z}. \tag{5}$$

Here,

$$s^2_Z c^2_Z = \frac{\pi\alpha_{em}}{\sqrt{2}G_F M^2_Z}, \tag{6}$$

where $\alpha_{em} = e^2/4\pi$ is the electromagnetic fine structure constant. We vary $\hat{x}$ between zero and $\hat{x} = 400$, with and without the form factor suppression of Eq. (3). For convenience of comparison with the literature, the values of $\hat{x}$ used in this paper translate as follows:

$$\hat{x} \ = 50 \Rightarrow \Delta\kappa = 0.13$$

$$\hat{x} \ = 200 \Rightarrow \Delta\kappa = 0.53$$

$$\hat{x} = 400 \Rightarrow \Delta\kappa = 1.06 \ . \tag{7}$$

Possible C or P violating terms are not included here as they are constrained by experimental measurements of the neutron electric dipole moment to be negligibly small compared to the non-CP violating anomalous couplings [18].

The Feynman rules for the $WW\gamma$ vertex from the Lagrangian of Eq. (1), with the momentum assignments $W_\beta(q) \to W_\mu(p_3) + \gamma_\nu(p_4)$, and setting $\lambda = 0$, give

$$\Gamma^{\rm SM}_{\beta\mu\nu}(q = p_3 + p_4, p_3, p_4) = \qquad - {\rm i}e\, Q_W \Big(g_{\beta\mu}(q + p_3)_\nu \\ - g_{\beta\nu}(q + p_4)_\mu + g_{\mu\nu}(p_4 - p_3)_\beta \Big) \tag{8}$$

$$\Gamma^{\rm NSM}_{\beta\mu\nu}(q = p_3 + p_4, p_3, p_4) = -{\rm i}e\, Q_W(\Delta\kappa) \Big(g_{\beta\nu} p_{4\mu} - g_{\mu\nu} p_{4\beta} \Big), \tag{9}$$

where $Q_W = \pm 1$ is the W charge.

B. Methodology

The calculations described here are the Born level, bremsstrahlung and $O(\alpha_s)$ corrections to $p\overline{p}$ and pp production of $W^\pm\gamma X$, to yield parton level results for $q_1\bar{q}_2 \to W^\pm\gamma$, $q_1\bar{q}_2 \to W^\pm\gamma g$ and $gq_1(\bar{q}_2) \to W^\pm g q_2(\bar{q}_1)$, in terms of a parton level differential cross section $d\hat{\sigma}$. The leading logarithm (LL) result includes the Born and bremsstrahlung contributions. The next-to-leading logarithmic (NLL) contributions include the interference of Born and virtual diagrams, the $O(\alpha_s)$ tree level corrections and NLL quark fragmentation into a photon. The parton differential cross sections are convoluted with the parton distribution functions $F_i^A(x_i, Q^2)$ for parton i and hadron A, and summed to yield the differential cross section

$$\mathrm{d}\sigma = \sum_{i,j} \int\int F_i^{(A)}\left(x_1, Q^2\right) F_j^{(B)}\left(x_2, Q^2\right) d\hat{\sigma}_{ij}\left(\alpha_s\left(\mu^2\right), Q^2\right) \mathrm{d}x_1 \mathrm{d}x_2 \ . \tag{10}$$

For the evaluation of the above integral, a combination of analytic and Monte Carlo techniques is employed. This method has been used in several processes, including the $W^{\pm}\gamma X$ process [13–15].

First, the collinear and soft divergences in the phase space are isolated by partitioning phase space with arbitrary (but small) cutoff parameters δ_s and δ_c. Next, the phase space integrals are performed analytically in $N = 4 - 2\epsilon$ dimensions where the collinear and soft gluon singularities appear as poles in ϵ. In the singular regions, the three body matrix elements are approximated using the soft gluon and leading pole approximations [19]. With the singularities of the two and three body matrix elements isolated, the soft singularities cancel the virtual singularities arising from loop integrals performed in calculating the virtual corrections. The collinear singularities are then factorized into the parton distribution functions. The Born, virtual, soft and collinear contributions are combined into what are called the two body matrix elements, since, at least approximately, they all have the same $2 \to 2$ kinematics. The tree level, non-singular contribution has $2 \to 3$ kinematics and is referred to as the three body contribution. The two and three body contributions are singularity free and may be integrated via standard Monte Carlo techniques. The separate two and three body contributions now depend on the theoretical soft and collinear cutoffs δ_s and δ_c, but when the two and three body contributions are combined, this dependence vanishes for a wide range of cutoff parameters.

The expressions for the two body matrix elements for the SM Lagrangian have been given in Ref. [13] and will not be given here. We do include in the Appendix the virtual corrections that involve the non-standard tri-boson coupling. The three body matrix elements are calculated with the helicity amplitude method detailed in Ref. [20] and references contained therein.

Photon bremsstrahlung contributions from final state radiation from a quark or antiquark are included via the inclusion of the NLL fragmentation functions for $q \to \gamma$ and $g \to \gamma$ as in Refs. [13] and [21]. A photon isolation cut requires that the sum of hadronic energy within a cone around the photon momentum be small. Quantitatively,

$$\sum_{\Delta R \leq 0.4} E_{had} < 0.15 E_\gamma \tag{11}$$

effectively suppresses the bremsstrahlung cross section [21]. Here, $\Delta R = [(\Delta\phi)^2 + (\Delta\eta)^2]^{1/2}$ is the cone size defined with respect to the photon pseudorapidity η and azimuthal angle ϕ.

Photons can arise from radiative W decay as well as from the production process. The signature of $W \to e\nu_e\gamma$ can, in principle, be separated from the production process experimentally by suitable kinematic cuts. In particular if a cut, $m_{\rm T}(\gamma\ell; \text{missing}) > 90$ Gev, is made on the cluster transverse mass variable

$$m^2_{\rm T}(\gamma\ell; \text{missing}) = \left[m^2_{\gamma\ell} + \mid \mathbf{p}_{\gamma \rm T} + \mathbf{p}_{\ell \rm T} \mid^2 + \mid \not{\mathbf{p}}_{\rm T} \mid\right]^2 - \mid \mathbf{p}_{\gamma \rm T} + \mathbf{p}_{\ell \rm T} + \not{\mathbf{p}}_{\rm T} \mid^2 \tag{12}$$

most of the radiative decay signal will be eliminated [7]. Here $\not{\mathbf{p}}_{\rm T}$ is the neutrino transverse momentum, which is missing in an experiment, and $\mathbf{p}_{\ell \rm T}$ is the lepton transverse momentum. In this calculation only the production process $p\overline{p}$ or $pp \to W^{\pm}\gamma X$ is considered for simplicity. The decay processes into leptons $\ell = e$ or $\ell = \mu$: $W \to \ell\nu_\ell$ and $W \to \ell\nu_\ell\gamma$ are ignored throughout, except as the branching fraction $BR(W \to \ell\nu_\ell)$ appears in event rates.

The strong coupling constant α_s is calculated at two loops for the NLL results and at one loop for the LL results, with the five light quark flavors contributing at their respective mass thresholds. Also, the HMRS set B structure functions [22] consistent with a NLL, $\overline{\rm MS}$ (Modified Minimal Subtraction scheme) calculation are used. For these structure functions, the four flavor value of $\Lambda_{\overline{\rm MS}}$ of 0.19 GeV is used. For convenience, we set the factorization scale equal to the renormalization scale. Unless otherwise specified, these scales are set to the $W\gamma$ invariant mass $M_{W\gamma}$. The electromagnetic fine structure constant at the Z mass scale $\alpha_{em} = 1/128.8$ is used. The narrow width approximation for the W propagator

$$\frac{1}{(s - M_W^2)^2 + M_W^2\Gamma_W^2} \approx \frac{\pi}{M_W\Gamma_W}\delta(s - M_W^2) \tag{13}$$

is also used.

In addition to the photon isolation cut described above, various kinematic cuts are imposed on the variables to simulate detector responses. The W and photon are both required to lie in a rapidity range of $|y| \leq 2.5$. A cut is made on the photon transverse momentum

to avoid the collinear and soft singularities arising from the parton level cross section. For the Tevatron, we select photons with $p_{\gamma\perp} > 10$ GeV, while at the LHC, we require $p_{\gamma\perp} > 50$ GeV.

III. RESULTS

The calculation described in Sec. II has been performed for $\sqrt{S} = 1.8$ TeV (Tevatron) and $\sqrt{S} = 14$ TeV (LHC) for $p\overline{p}$ and pp, respectively. In the tables and figures presented below, the number of events, N, is obtained from

$$N = \mathcal{L} \times BR \times \int_{p_{1\gamma\perp}}^{p_{2\gamma\perp}} \frac{\mathrm{d}\sigma}{\mathrm{d}p_{\gamma\perp}} \mathrm{d}p_{\gamma\perp} \tag{14}$$

where $BR \approx 0.2$ is the sum of the electronic and muonic branching fractions for the W, $\mathcal{L}$ is the integrated luminosity $\mathcal{L} = \int L dt$ over a collider year, and $\mathrm{d}\sigma/\mathrm{d}p_{\gamma\perp}$ is the $|\mathbf{p}_{\gamma\perp}|$ spectrum of the photon. The calculations are performed with various values of $\hat{x} = 0$, 50, 200, 400, and with different regions of $p_{\gamma\perp}$. The value of $\hat{x} = 0$ corresponds to the SM. The integrated luminosity for the Tevatron is taken as $\mathcal{L} = 100$ pb^{-1}, while the LHC luminosity used is $\mathcal{L} = 3 \times 10^4$ pb^{-1}. For the pp collider the event rates for W^+ are slightly higher than for W^-, while at the $p\bar{p}$ collider the event rates for $W^\pm$ are the same.

A. Tevatron Collider

We begin with a comparison of the LL event rates along with the NLL values. These calculations for the Tevatron Collider are presented in Tables 1 and 2. The trends are evident in the tables. At the Tevatron, with no form factors, the LL and NLL event rates are enhanced with increasing $\hat{x}$. The amount of increase is small, however, for low $p_{\gamma\perp}$. At the leading log level, the difference from $\hat{x} = 0$ to $\hat{x} = 400$ is only 14 events at 10 GeV $\leq$ $p_{\gamma\perp}$ $\leq$ 50 GeV. This corresponds to a 10% increase. At 50 GeV $\leq$ $p_{\gamma\perp}$ $\leq$ 150 GeV, the increase is from 6 to 14 events. The SM signal is enhanced by about 25% when the NLL corrections are included at the low $p_{\gamma\perp}$ end. At the high $p_{\gamma\perp}$ end, the increase is 50%, but this only means an increase of 3 events, not statistically significant given the associated statistical uncertainty. All of this can be seen qualitatively by examining the photon transverse momentum spectra shown in Figs. 1 (LL) and 2 (NLL), where we show

$\mathrm{d}\sigma(p\bar{p} \to W^+\gamma X)/\mathrm{d}p_{\gamma\perp}$ at the Tevatron. The anomalous $WW\gamma$ coupling enhances the high $p_{\gamma\perp}$ tail of the distributions. No form factors are used for the distributions.

Tables 1 and 2 indicate that the event rates at the Tevatron are nearly equal with and without form factors, for both LL and NLL results. This is due to the fact that $M^2_{W\gamma}/\Lambda^2$ in the form factor is small. The differences in number of events are not statistically significant, although the form factor approach does decrease the number of events. Thus, limits obtained including the form factor suppression could be considered to be conservative.

The D0 Collaboration reports a value of $-2.5 \leq \Delta\kappa \leq 2.7$ [2] from a data sample of approximately 15 pb^{-1} from the 1992/93 run. The limits are set using the NSM enhancement in the total cross section. To estimate the sensitivity at an integrated luminosity of 100 pb^{-1}, we consider the high $p_{\gamma\perp}$ region in Table 2. We see from Table 2 that a doubling of the SM event rate from 9 to 18 events for 50 GeV$\leq p_{\gamma\perp} \leq$150 GeV occurs at $\hat{x} \simeq 400$. For comparable values of $\hat{x}$, it would be difficult to set a limit from the cross section alone because the NSM enhancement of the cross section is not very large, less than 10% for $\hat{x} = 400$. From Eq. (7), this corresponds to $\Delta\kappa \simeq 1$.

Baur, Han and Ohnemus in Ref. [14] have estimated a sensitivity to $|\Delta\kappa| \simeq 1.6$ at the 2σ level and $|\Delta\kappa| \simeq 0.9$ at the 1σ level for an integrated luminosity of 100 pb^{-1} at the Tevatron. Their results for positive and negative $\Delta\kappa$ are approximately equal. They take $p_{\gamma\perp} > 10$ GeV, and impose a variety of other cuts including those on the leptons from the W decay. From Tables 1 and 2 combined, we see that the enhancement of the NLL over the LL results is approximately constant as a function of $\hat{x}$ when one includes $p_{\gamma\perp} > 10$ GeV. Since the form factor has at most a few percent effect in the direction of suppressing the nonstandard contributions, the Tevatron results of Ref. [14] can be carried over to the case where no form factors are used. A value of $\Delta\kappa = 1.6$ corresponds to $\hat{x} \simeq 600$. The limits of Ref. [14] apply to $\Delta\kappa$ for any value of λ in Eq. (1), so with $\lambda = 0$, the limits on $\Delta\kappa$ improve somewhat, an estimated 10–30% [12].

B. Large Hadron Collider

At the LHC, the results are somewhat different than for the Tevatron. The discussion will cover only the case of $W^+\gamma$ production, with similar conclusions for $W^-\gamma$ production. As with the Tevatron Collider, as $\hat{x}$ increases, so does the cross section because of a flatter $p_{\gamma\perp}$ distribution. Event rates for $\sqrt{S} = 14$ TeV for two ranges of $p_{\gamma\perp}$ are shown in Table 3 (200 GeV$\leq p_{\gamma\perp} \leq$ 400 GeV) and Table 4 (400 GeV$\leq p_{\gamma\perp} \leq$ 750 GeV), using the cuts described in Sec. II. Our results for large $\hat{x}$ at the LHC indicate that the cross section scales approximately as $\hat{x}^2$. We use this approximate $\hat{x}^2$ dependence to extrapolate between values of $\hat{x}$ given in Tables 3 and 4. In addition, our conclusions should be valid for positive and negative $\hat{x}$. The LHC results, because of the significantly higher energy at the LHC, exhibit two striking features. First, as has been pointed out in the literature [13–15], the QCD corrections are enormous. Second, the form factor results are measurably lower than the results with no form factor.

Tables 3 and 4 demonstrate that the QCD corrections overwhelm the SM LL signal at the LHC, being as much as five times the LL signal at low $p_{\gamma\perp}$, and increasing to seven times the LL signal at the high $p_{\gamma\perp}$ end of the spectrum in the SM. These large contributions at $\mathcal{O}(\alpha_s)$ would seem to cast doubt on the validity of the perturbative expansion, but are generally caused by the presence of the radiation zero mentioned above, thereby suppressing the photon transverse momentum distributions at LL order [13]. The transverse momentum distributions at LL and NLL for $pp \to W^+\gamma X$ at the LHC, without form factor suppression, are shown in Figs. 3 and 4. Ref. [14] describes a method to reduce QCD effects in $W\gamma$ production by putting appropriate cuts on the final state parton that appears in the $O(\alpha_s)$ tree level matrix element. This effectively reduces the large contributions from the $\mathcal{O}(\alpha_s)$ corrections, but also reduces the event rate. Such cuts will not be considered here. Instead, we consider the quantity

$$\frac{\sigma(p_{\gamma\perp} > p_{\gamma\perp\min})}{\sigma(p_{\gamma\perp} > 50 \text{ GeV})} \ , \tag{15}$$

where some of the QCD uncertainties cancel in the ratio.

In Fig. 5, we show the cross section ratios for the standard model at LL and NLL and the NSM results at NLL for $\hat{x} = 50$, 200 and 400. The ratio reflects the significant increase in events at high $p_{\gamma\perp}$ due to the QCD and NSM effects seen in Figs. 3 and 4. We have put in error bars to indicate the statistical errors given an integrated luminosity of 3×10^4 pb^{-1}, including the branching fractions for $W \to e$ and $W \to \mu$. The $\hat{x} = 50$ signal is a 1σ distance from the SM for the $p_{\gamma\perp} \gtrsim 400$ GeV. For Fig. 5, the factorization and renormalization scales Q are kept at a value of $Q = M_{W\gamma}$. Fig. 6 shows the cross section ratios as a function of $p_{\gamma\perp\min}$, at NLL, for three values of Q. The spread in the ratio stays within the statistical error bars, but the QCD uncertainty is large enough to make a limit of $\hat{x} \sim 50$ difficult without additional cuts invoked [23].

The analysis of Falk, Luke and Simmons [6] of the sensitivity of the LHC to $\hat{x} \neq 0$ used the number of excess events in the high $p_{\gamma\perp}$ range, at leading order, as a guide to LHC sensitivity. They required a doubling of the standard model event rate. Table 4 indicates that the LHC would be sensitive to $\hat{x} \simeq 50$ at leading order with this criterion. This is roughly the conclusion of Ref. [6] in their $W\gamma$ discussion for a higher LHC energy but lower integrated luminosity. At NLL, however, the same criterion means a sensitivity to $\hat{x} \sim 140$. An alternative way to assess the importance of the QCD corrections is to compare the standard model NLL rate with the nonstandard model LL rate. The number of predicted events for 400 GeV $\leq p_{\gamma\perp} \leq$ 700 GeV at the LHC is equivalent, at LL, to a value of $\hat{x} \sim 140$.

We now turn to the issue of form factor suppression of NSM effects. Tables 3 and 4, and Figs. 7 and 8 indicate the degree to which the form factor suppresses the cross section. Figs. 7 and 8 show the LL and NLL $p_{\gamma\perp}$ distributions. In these figures as well as the form factor results in the tables, the form factor of Eq. (3) is used with $\Lambda = 1$ TeV and $n = 2$. With form factors applied, the increases in Table 3 from the SM are a bit more modest than without the form factor: the SM LL event rate increases roughly by a factor of five for $\hat{x} = 400$, and the NLL increase is less than twice the SM at the same value of $\hat{x}$. At high $p_{\gamma\perp}$, 400 GeV $\leq p_{\gamma\perp} \leq 700$ GeV with no form factors applied the increases from the SM values for LL and NLL are sixty and ten respectively for $\hat{x} = 400$. With form factors

applied, the increase from $\hat{x} = 0$ to $\hat{x} = 400$ for LL is about five times the SM value. At NLL the increase from SM and $\hat{x} = 400$ is a relatively modest 17%.

Because the form factor depends on $M_{W\gamma}$, the translation between results with and without form factors is not completely straightforward. From Table 3, where 200 GeV$\leq$ $p_{\gamma\perp} \leq$ 400 GeV, the number of events with the form factor applied at $\hat{x} = 400$ is equivalent to the number of events predicted without form factors at $\hat{x} \simeq 200$. In this range of $p_{\gamma\perp}$, the average value of $M_{W\gamma}$ is $< M_{W\gamma} >\sim$600 GeV, which accounts for the suppression. At larger values of $p_{\gamma\perp}$, the suppression is stronger. In Table 4, the event rate for $\hat{x} = 400$ with the form factor is equivalent to $\hat{x} \simeq 150$ without form factor suppression. At lower values of $p_{\gamma\perp}$, the form factor is less important. For 100 GeV$\leq p_{\gamma\perp} \leq$ 200 GeV, $< M_{W\gamma} >\simeq$ 330 GeV. From this, we estimate that $\hat{x} = 400$ with form factor multiplication is equivalent to $\hat{x} \simeq 325$ in this $p_{\gamma\perp}$ bin, effectively a factor of 0.8 lower in the $\hat{x}$ value.

We use these comparisons to translate the sensitivity limits of Baur, Han and Ohnemus in Ref. [14] to limits without form factors. In Ref. [14], the inclusive NLL distributions are used to set sensitivity limits of $\Delta\kappa \sim 0.3$ at 1σ and $\Delta\kappa \sim 0.5$ at 2σ at $\sqrt{S} = 40$ TeV for the Superconducting Super Collider, for any value of λ in Eq. (1). They comment that the LHC limits are larger by a factor of ~ 1.5. In terms of $\hat{x}$, this means a sensitivity (with form factors) of $\hat{x} \sim 180 - 300$ for the 1–2σ range. Their analysis involves a variety of cuts, including cuts on the leptons as well as $p_{\gamma\perp} \geq 100$ GeV. Since low $p_{\gamma\perp}$ dominates the cross section, a conservative estimate, using the multiplicative factor of 0.8, would be that the LHC is sensitive to $\hat{x} \sim 150 - 250$ in the absence of form factors in the calculation. A less conservative estimate would be to take the factor of 0.5 found from the range of 200–400 GeV for $p_{\gamma\perp}$ to yield 90–150 for $\hat{x}$ when form factors are taken out of the analysis.

We comment that Baur *et al.* have also considered the next-to-leading order $W\gamma + 0$-jet rate, as a way to eliminate some of the QCD uncertainties. The inclusive NLL limits are a factor of 1.2-1.5 higher than those obtained with the no-jet rate [14]. In addition, they use an integrated luminosity of 10^4 pb^{-1} and only include the W^+ production with $W \to e\nu_e$ decay channel, and comment that the limits can be improved by 20–40% with the inclusion

of W^- and $W \to \mu\nu_\mu$. By accounting for these improvements and an integrated luminosity of 3×10^4 pb^{-1}, one is led to a lower limit on $\hat{x}$: at best $\hat{x} \sim 150 - 250$ is reduced to $\hat{x} \sim 80 - 140$.

IV. CONCLUSIONS

A comparison sensitivity limits with and without form factors, including QCD corrections, has been done for the NSM parameter $\hat{x} > 0$, which also applies to negative values of $\hat{x}$. We have demonstrated that QCD corrections and form factor suppression have significantly different effects at Tevatron and LHC energies. At the Tevatron, QCD corrections are at the level of $\sim 35\%$ of the Born cross section. The form factor suppression at the Tevatron is essentially negligible, so the results of Ref. [14], which include QCD corrections, can be carried over to the effective Lagrangian approach. Their estimated sensitivity to the nonstandard coupling is at $\hat{x} \sim 360 - 600$, the range of $\Delta\kappa \simeq 0.9$ at the 1σ level and $\Delta\kappa \simeq 1.6$ at the 2σ level. Our cruder estimate, requiring a doubling of the SM events for 50 GeV $\leq p_{\gamma\perp} \leq$ 150 GeV, yields a comparable value of $\hat{x} = 400$.

At the LHC, however, the QCD corrections play a much more important role in the sensitivity limits. Doubling the number of events at LL, for 400 GeV$\leq p_{\gamma\perp} \leq$ 700 GeV occurs for $\hat{x} \simeq 50$, while at NLL, for the same range of $p_{\gamma\perp}$, a value of $\hat{x} \simeq 140$ is required. The more complete analysis of Ref. [14], done with form factors and a variety of theoretical cuts, can be translated to effective Lagrangian results by evaluating $< M_{W\gamma} >$. We estimate that the limits of Ref. [14] translate to a sensitivity to $\hat{x} \simeq 150 - 250$ without form factors, although it is possible that these limits could be reduced somewhat.

Each collider energy has its advantages, however, the conclusion that we must draw is that neither the Tevatron with $\mathcal{L} = 100$ pb^{-1} nor the LHC with $\mathcal{L} = 3 \times 10^4$ pb^{-1} will be sensitive to values of the anomalous $WW\gamma$ coupling $\hat{x}$ that are relevant to the effective Lagrangian approach. With the definition of $\hat{x}$ in Eq. (2.5), the value of $\hat{x}$ in the effective Lagrangian is naively expected to be of order unity [6]. If values of $\hat{x} \sim 100$ were measured in

experiments, one would bring into question the validity of the effective Lagrangian approach where only one nonstandard coupling is kept in the $WW\gamma$ effective Lagrangian. This is the same conclusion for the $WW\gamma$ anomalous coupling reached in Ref. [6] with a leading order analysis. Our results are more pessimistic, because using the same criterion, a doubling of events at high $p_{\gamma\perp}$, the inclusion of QCD effects weakens the estimate in Ref. [6] of the LHC sensitivity to $\hat{x}$ by a factor of $2-3$.

ACKNOWLEDGMENTS

We thank U. Baur for discussions. This work was supported in part by NSF Grants No. PHY-9104773 and No. PHY-9307213.

VIRTUAL APPENDIX

The matrix element squared for the one loop virtual correction to $q_1(p_1) + \bar{q}_2(p_2) \rightarrow W(p_3) + \gamma(p_4)$ is written in terms of Mandelstam invariants

$$s = (p_1 + p_2)^2 \quad t = (p_1 - p_4)^2 \quad u = (p_2 - p_4)^2 \ . \tag{16}$$

It has the form

$$\sum_{avg} |M_V|^2 = \frac{1}{9}\frac{1}{4}\frac{e^4}{2\sin^2\theta_W} N_C \frac{\alpha_s}{2\pi}\left(\frac{4\pi\mu^2}{M_W^2}\right)^{\epsilon}\frac{\Gamma(1-\epsilon)}{\Gamma(1-2\epsilon)} C_F$$

$$\cdot \left[F_V(s,t,u,\epsilon) + G_V(s,t,u,\epsilon)\right] \tag{17}$$

F_V is the standard model contribution and it is explicitly written out in Ref. [13]. We have check that Ohnemus' expression is correct. The NSM contribution to the virtual correction appears in G_V, which is written in terms of the NSM part of the Born matrix element squared

$$T_1 = \frac{(Q_1 - Q_2)^2}{2M_W^2(t+u)^2}(\Delta\kappa)^2\Big[s(t+u)^2(1-\epsilon) + 4tu(t+u)(1-\epsilon)$$

$$+ 2stu(1-2\epsilon)\Big] \tag{18}$$

$$T_2 = \frac{(Q_1-Q_2)(Q_1u+Q_2t)}{(t+u)^2} 4(t-u)(\Delta\kappa)(1-\epsilon) \tag{19}$$

We calculate the NSM virtual correction to be

$$\begin{aligned} G_V(s,t,u,\epsilon) = {} & [T_1(s,t,u,\epsilon)+T_2(s,t,u,\epsilon)]\Big(\frac{s}{M_W^2}\Big)^{-\epsilon}\Big(-\frac{2}{\epsilon^2}-\frac{3}{\epsilon}+\frac{2}{3}\pi^2\Big) \\ & + \mathcal{F}(Q_1,Q_2,s,t,u) + \mathcal{F}(Q_2,Q_1,s,u,t) \end{aligned} \tag{20}$$

where

$$\begin{aligned} \mathcal{F}(Q_1,Q_2,s,t,u) = {} & \frac{Q_1(Q_1-Q_2)}{t+u}(\Delta\kappa)\Bigg[4F_1(s,t)(M_W^2-t) \\ & + \ln^2\Big(\frac{s}{M_W^2}\Big)\Big(3u+t-\frac{1}{M_W^2}(t^2+u^2+ut)\Big) \\ & + 4\ln\Big(\frac{|t|}{M_W^2}\Big)\frac{u}{2}\Big(2-\frac{t+u}{s+u}-\frac{M_W^2u}{(s+u)^2}+\frac{3t}{s+u}\Big) \\ & + 2u\Big(-\frac{u}{s+u}+7-10\frac{t}{t+u}\Big) \\ & + 4(\Delta\kappa)\Big(-\frac{s(t+u)}{M_W^2}-2tu(\frac{1}{t+u}+\frac{1}{M_W^2})\Big) \\ & + 2\ln\Big(\frac{s}{M_W^2}\Big)\Big(M_W^2-t+\frac{2M_W^2u}{t+u}\Big)\Bigg] \\ & + \frac{(Q_1u+Q_2t)(Q_1-Q_2)}{(t+u)^2}(\Delta\kappa)\Bigg[11-\ln^2\Big(\frac{s}{M_W^2}\Big)\Bigg](u-t) \\ & - (Q_1-Q_2)^2\frac{1}{2}\ln^2\Big(\frac{s}{M_W^2}\Big)(\Delta\kappa)\Bigg[1+\frac{4tu}{(t+u)^2}-\frac{u^2+t^2+ut}{M_W^2(t+u)}\Bigg] \end{aligned} \tag{21}$$

with the function F_1 defined as

$$\begin{aligned} F_1(s,t) = {} & \ln\Big(\frac{s}{M_W^2}\Big)\ln\Big(\frac{t}{M_W^2-s}\Big)+\frac{1}{2}\ln^2\Big(\frac{M_W^2}{s}\Big)-\frac{1}{2}\ln^2\Big(\frac{M_W^2-t}{M_W^2}\Big) \\ & + \mathrm{Li}_2\Big(\frac{M_W^2}{s}\Big)-\mathrm{Li}_2\Big(\frac{M_W^2}{M_W^2-t}\Big)\ . \end{aligned} \tag{22}$$

REFERENCES

[1] J. Alitti *et al.* (UA2 Collaboration), Phys. Lett. **B277**, 194 (1992).

[2] A. L. Spadafora *et al.* (D0 Collaboration), Fermilab preprint FERMILAB-CONF-94-016-E, to appear in the Proceedings of the 9th Topical Workshop on $\bar{p}p$ Collider Physics, Tsukuba, Japan, October 1993.

[3] Th. Müller (CDF Collaboration), UCLA preprint UCLA-PPH0058-11/93, to appear in the Proceedings of the Europhysics Conference on High Energy Physics, Marseille, France, July 1993.

[4] K. O. Mikaelian, M. A. Samuel and D. Sahdev, Phys. Rev. Lett. **43**, 746, 1979.

[5] U. Baur, T. Han and J. Ohnemus, Florida State University preprint FSU-HEP-940307 (March 1994).

[6] A. Falk, M. Luke and E. Simmons, Nucl. Phys. **B365**, 523 (1991).

[7] J. Cortes, K. Hagiwara and F. Herzog, Nuc. Phys. **B278**, 26 (1986).

[8] U. Baur and D. Zeppenfeld, Nucl. Phys. **B308**, 127 (1988).

[9] U. Baur and E. Berger, Phys. Rev. **D41**, 1476 (1990); Phys. Rev. **D47**, 4889 (1993).

[10] J. Smith, D. Thomas and W. L. van Neerven, Zeit. Phys. **C44**, 267 (1989).

[11] U. Baur, E. W. N. Glover and J. J. van der Bij, Nucl. Phys. **B318**, 106 (1989).

[12] U. Baur, S. Errede and J. Ohnemus, Phys. Rev. **D48**, 4103 (1993).

[13] J. Ohnemus, Phys. Rev. **D47**, 940 (1993).

[14] U. Baur, T. Han and J. Ohnemus, Phys. Rev. **D48**, 5140 (1993).

[15] S. Mendoza and J. Smith, SUNY, Stony Brook preprints ITP-SB-93-72 and ITP-SB-93-80; S. Mendoza, J. Smith and W. L. van Neerven, Phys. Rev. **D47**, 3913 (1993).

[16] R. E. Taylor *Proc. 1975 Int. Symp. on Lepton and Photon Interactions at High Energy* (ed. W. T. Kirk).

[17] A. Longhitano, Nucl. Phys. **B188**, 118 (1981).

[18] W. J. Marciano and A. Queijeiro, Phys. Rev. **D33**, 3449 (1986).

[19] L. Bergmann, Ph.D. thesis, Florida State University, FSU-HEP-890215 (unpublished).

[20] V. Barger, T. Han and D. Zeppenfield, Phys. Rev. **D41**, 2782 (1990).

[21] J. Ohnemus and W. J. Stirling, Phys. Lett. **B298**, 230 (1993).

[22] P. Harriman, A. Martin, R. Roberts, W. Stirling, Phys. Rev **D42**, 798 (1990).

[23] See, for example, Ref. [14] for a discussion of cuts to reduce the QCD contributions.

Table 1. Events for $\sqrt{S} = 1.8$ TeV ; 10 GeV $\leq |\ \mathbf{p}_{\gamma\perp}\ | \leq 50$ GeV
LL = Leading Log ; NFF = No Form Factors ; FF = Form Factors

	SM	$\hat{x} = 50$	$\hat{x} = 200$	$\hat{x} = 400$
W^+(LL,NFF)	142	142	147	156
W^+(LL,FF)	142	142	146	156
W^+(NLL,NFF)	193	194	200	206
W^+(NLL,FF)	193	190	195	210

Table 2. Events for $\sqrt{S} = 1.8$ TeV ; 50 GeV $\leq |\ \mathbf{p}_{\gamma\perp}\ | \leq 150$ GeV
LL = Leading Log ; NFF = No Form Factors ; FF = Form Factors

	SM	$\hat{x} = 50$	$\hat{x} = 200$	$\hat{x} = 400$
W^+(LL,NFF)	6	6	8	14
W^+(LL,FF)	6	6	8	13
W^+(NLL,NFF)	9	9	11	18
W^+(NLL,FF)	9	9	11	16

Table 3. Events for $\sqrt{S} = 14$ TeV ; 200 GeV $\leq |\, \mathbf{p}_{\gamma\perp} \,| \leq$ 400 GeV
LL = Leading Log ; NFF = No Form Factors ; FF = Form Factors

	SM	$\hat{x} = 50$	$\hat{x} = 200$	$\hat{x} = 400$
W^+(LL,NFF)	398	495	1788	5875
W^+(LL,FF)	398	425	773	1837
W^-(LL,NFF)	306	367	1191	3786
W^-(LL,FF)	306	325	549	1250
W^+(NLL,NFF)	1998	2007	3147	7314
W^+(NLL,FF)	1998	1949	2117	3138
W^-(NLL,NFF)	1364	1363	2112	4786
W^-(NLL,FF)	1364	1338	1463	2103

Table 4. Events for $\sqrt{S} = 14$ TeV ; 400 GeV $\leq |\, \mathbf{p}_{\gamma\perp} \,| \leq$ 700 GeV
LL = Leading Log ; NFF = No Form Factors ; FF = Form Factors

	SM	$\hat{x} = 50$	$\hat{x} = 200$	$\hat{x} = 400$
W^+(LL,NFF)	34	64	498	1890
W^+(LL,FF)	34	35	59	132
W^-(LL,NFF)	21	36	258	969
W^-(LL,FF)	21	22	34	72
W^+(NLL,NFF)	236	258	724	2258
W^+(NLL,FF)	236	228	228	283
W^-(NLL,NFF)	130	140	370	1178
W^-(NLL,FF)	130	127	122	152

FIGURES

FIG. 1. The LL photon transverse momentum distribution $\mathrm{d}\sigma(p\bar{p} \to W^+\gamma X)/\mathrm{d}p_{\gamma\perp}$ at $\sqrt{S} = 1.8$ TeV for $\hat{x} = 0,\ 50,\ 200$ and 400. The figure includes Born term and bremsstrahlung contributions with the cuts described in Sec. II of the text. No form factors are used to reduce the cross section.

FIG. 2. The NLL photon transverse momentum distribution at $\sqrt{S} = 1.8$, as in Fig. 1.

FIG. 3. The LL $p_{\gamma\perp}$ distributions for $pp \to W^+\gamma X$ at $\sqrt{S} = 14$ TeV for $\hat{x} = 0,\ 50,\ 200$ and 400. The figure includes Born term and bremsstrahlung contributions with the cuts described in Sec. II of the text. No form factors are used to reduce the cross section.

FIG. 4. Same as in Fig. 3, now including NLL contributions.

FIG. 5. Cross section ratios $\sigma(p_{\gamma\perp} > p_{\gamma\perp\mathrm{min}})/\sigma(p_{\gamma\perp} > 50\ \mathrm{GeV})$ for the LHC with the cuts described in Sec. II. Shown are curves for the SM at LL and NLL results for $\hat{x} = 0,\ 50,\ 200,\ 400$. The error bars are an estimate of the statistical errors using a leptonic branching fraction $BR = 0.20$ and integrated luminosity $\mathcal{L} = 3 \times 10^4\ \mathrm{pb}^{-1}$. No form factors are applied.

FIG. 6. The NLL standard model values for $\sigma(p_{\gamma\perp} > p_{\gamma\perp\mathrm{min}})/\sigma(p_{\gamma\perp} > 50\ \mathrm{GeV})$ as a function of $p_{\gamma\perp\mathrm{min}}$, for $Q = M_{W\gamma}$, $Q = \frac{1}{2}\sqrt{M_{W\gamma}^2 + p_{W\gamma}^2}$ and $Q = \sqrt{\hat{s}}$.

FIG. 7. The same LL plots at the LHC as in Fig. 3 but with the form factors of Eq. (3) with $\Lambda = 1$ TeV and $n = 2$ applied.

FIG. 8. The same plots as Fig. 7, including the form factor, now at NLL.

This figure "fig1-1.png" is available in "png" format from:

http://arXiv.org/ps/hep-ph/9406331v1

This figure "fig2-1.png" is available in "png" format from:

http://arXiv.org/ps/hep-ph/9406331v1

This figure "fig1-2.png" is available in "png" format from:

http://arXiv.org/ps/hep-ph/9406331v1

This figure "fig2-2.png" is available in "png" format from:

http://arXiv.org/ps/hep-ph/9406331v1

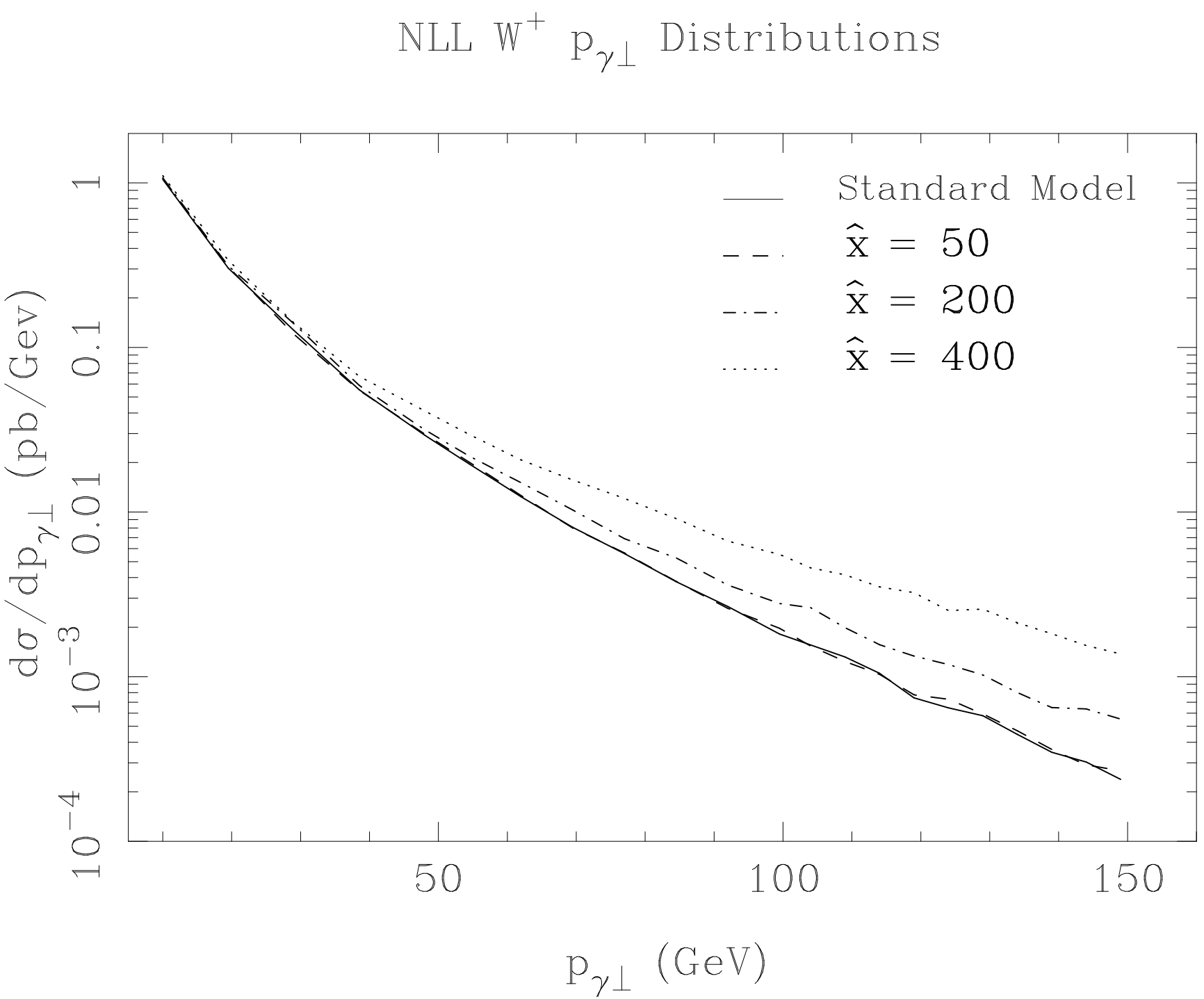
NLL W^+ $p_{\gamma\perp}$ Distributions
Standard Model
$\hat{x}$ = 50
$\hat{x}$ = 200
$\hat{x}$ = 400
$d\sigma/dp_{\gamma\perp}$ (pb/Gev)
10^{-4}
10^{-3}
0.01
0.1
1
50
100
150
$p_{\gamma\perp}$ (GeV)

Figure 2

This figure "fig1-3.png" is available in "png" format from:

http://arXiv.org/ps/hep-ph/9406331v1

This figure "fig2-3.png" is available in "png" format from:

http://arXiv.org/ps/hep-ph/9406331v1

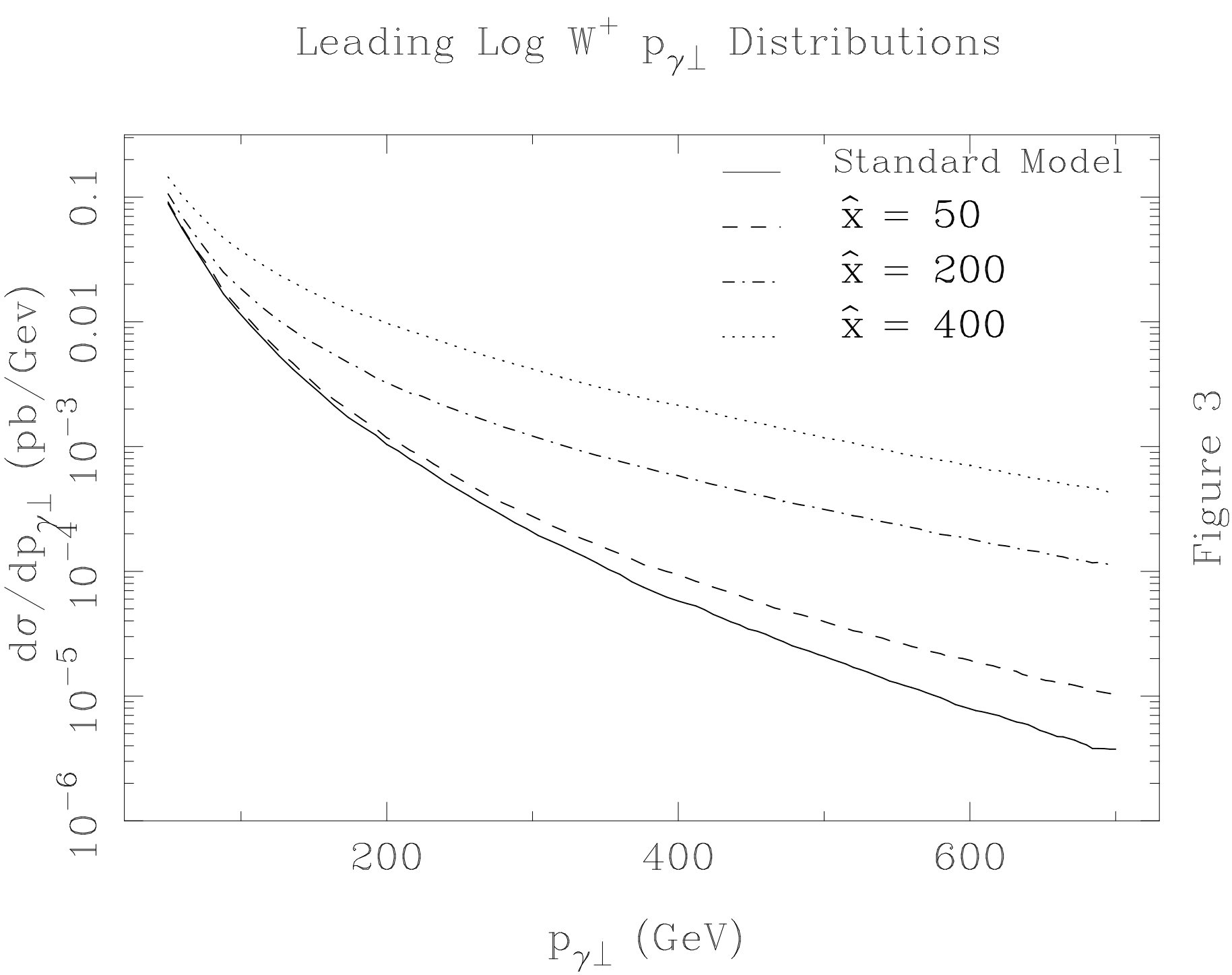
Leading Log W^+ $p_{\gamma\perp}$ Distributions
Standard Model
$\hat{x}$ = 50
$\hat{x}$ = 200
$\hat{x}$ = 400
$d\sigma/dp_{\gamma\perp}$ (pb/Gev)
10^{-6} 10^{-5} 10^{-4} 10^{-3} 0.01 0.1
200 400 600
$p_{\gamma\perp}$ (GeV)

Figure 3

This figure "fig1-4.png" is available in "png" format from:

http://arXiv.org/ps/hep-ph/9406331v1

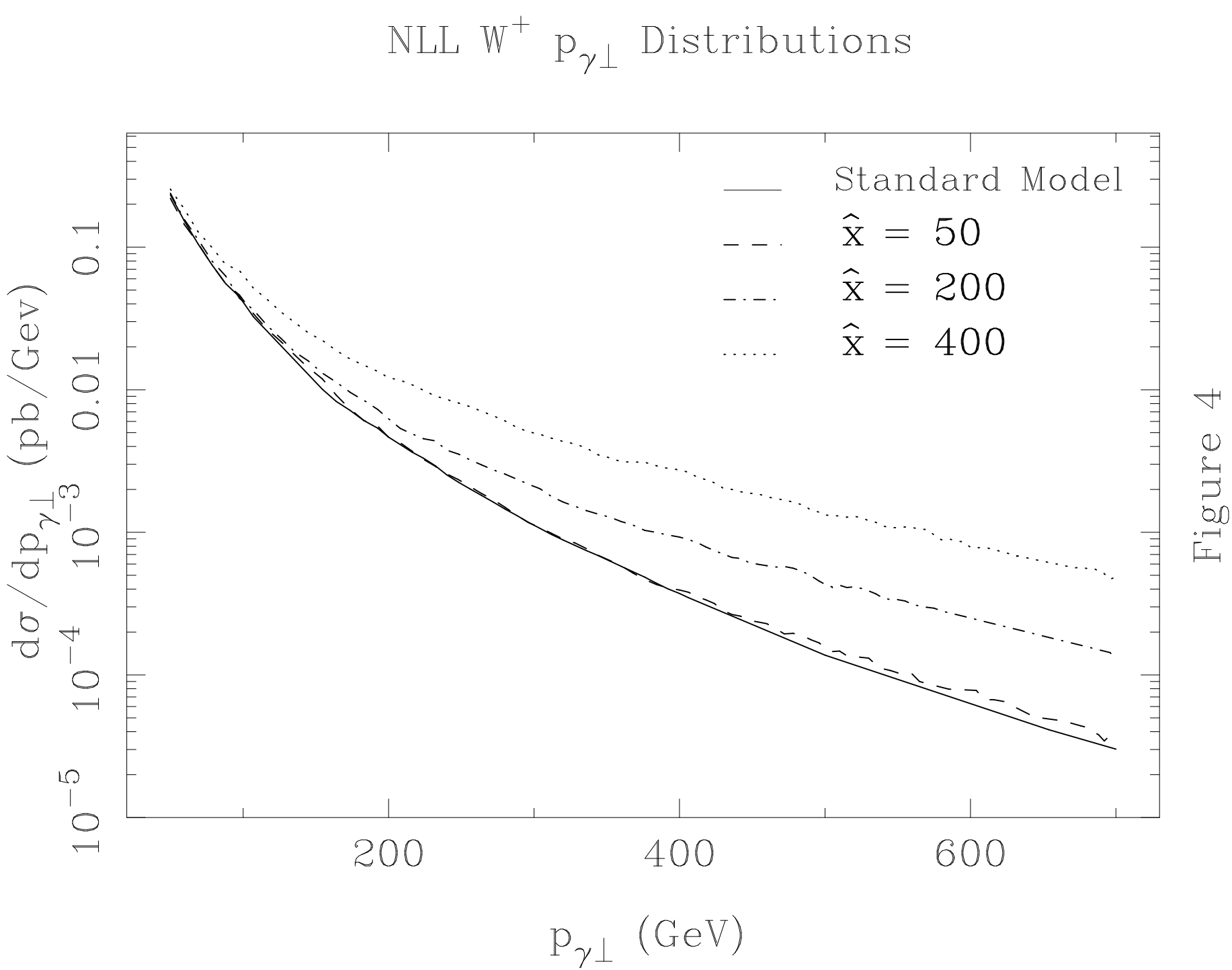
NLL W^+ $p_{\gamma\perp}$ Distributions
Standard Model
$\hat{x}$ = 50
$\hat{x}$ = 200
$\hat{x}$ = 400
$d\sigma/dp_{\gamma\perp}$ (pb/Gev)
10^{-5}
10^{-4}
10^{-3}
0.01
0.1
200
400
600
$p_{\gamma\perp}$ (GeV)

Figure 4

This figure "fig1-5.png" is available in "png" format from:

http://arXiv.org/ps/hep-ph/9406331v1

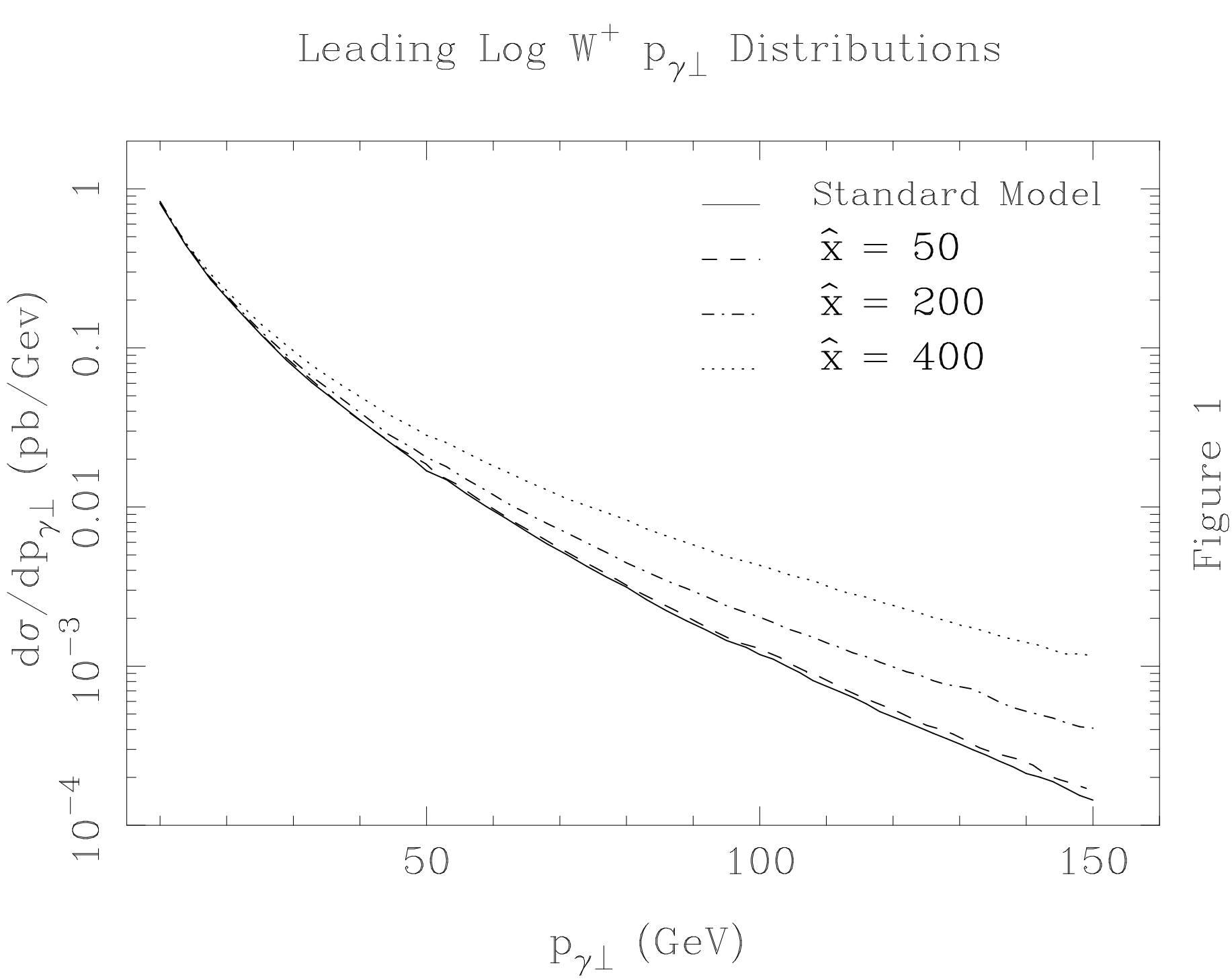
Leading Log W^+ $p_{\gamma\perp}$ Distributions
Standard Model
$\hat{x}$ = 50
$\hat{x}$ = 200
$\hat{x}$ = 400
$d\sigma/dp_{\gamma\perp}$ (pb/Gev)
1
0.1
0.01
10^{-3}
10^{-4}
50
100
150
$p_{\gamma\perp}$ (GeV)

Figure 1

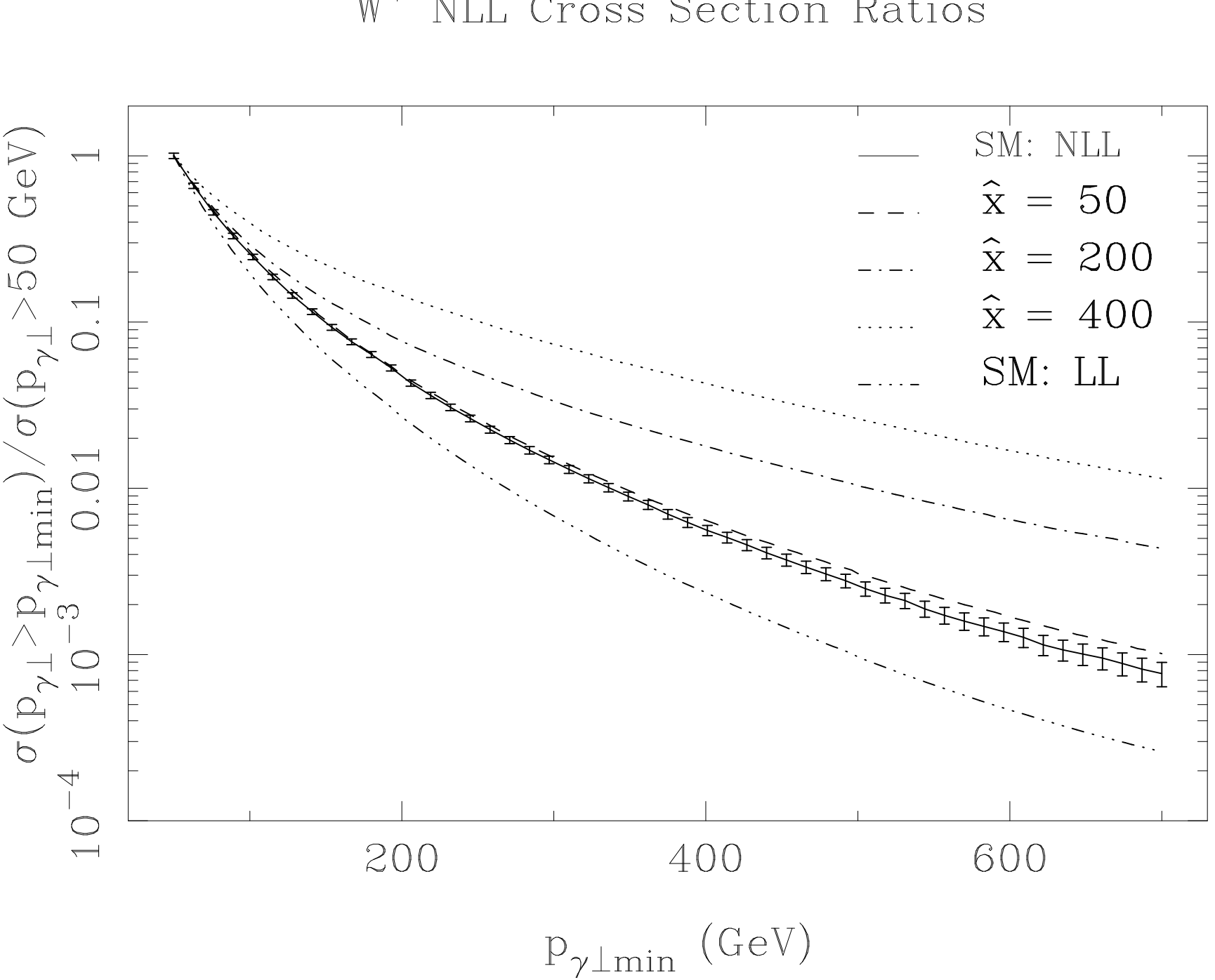
W+ NLL Cross Section Ratios
SM: NLL
x̂ = 50
x̂ = 200
x̂ = 400
SM: LL
σ(pγ⊥>pγ⊥min)/σ(pγ⊥>50 GeV)
10−4
10−3
0.01
0.1
1
200
400
600
pγ⊥min (GeV)

Figure 5

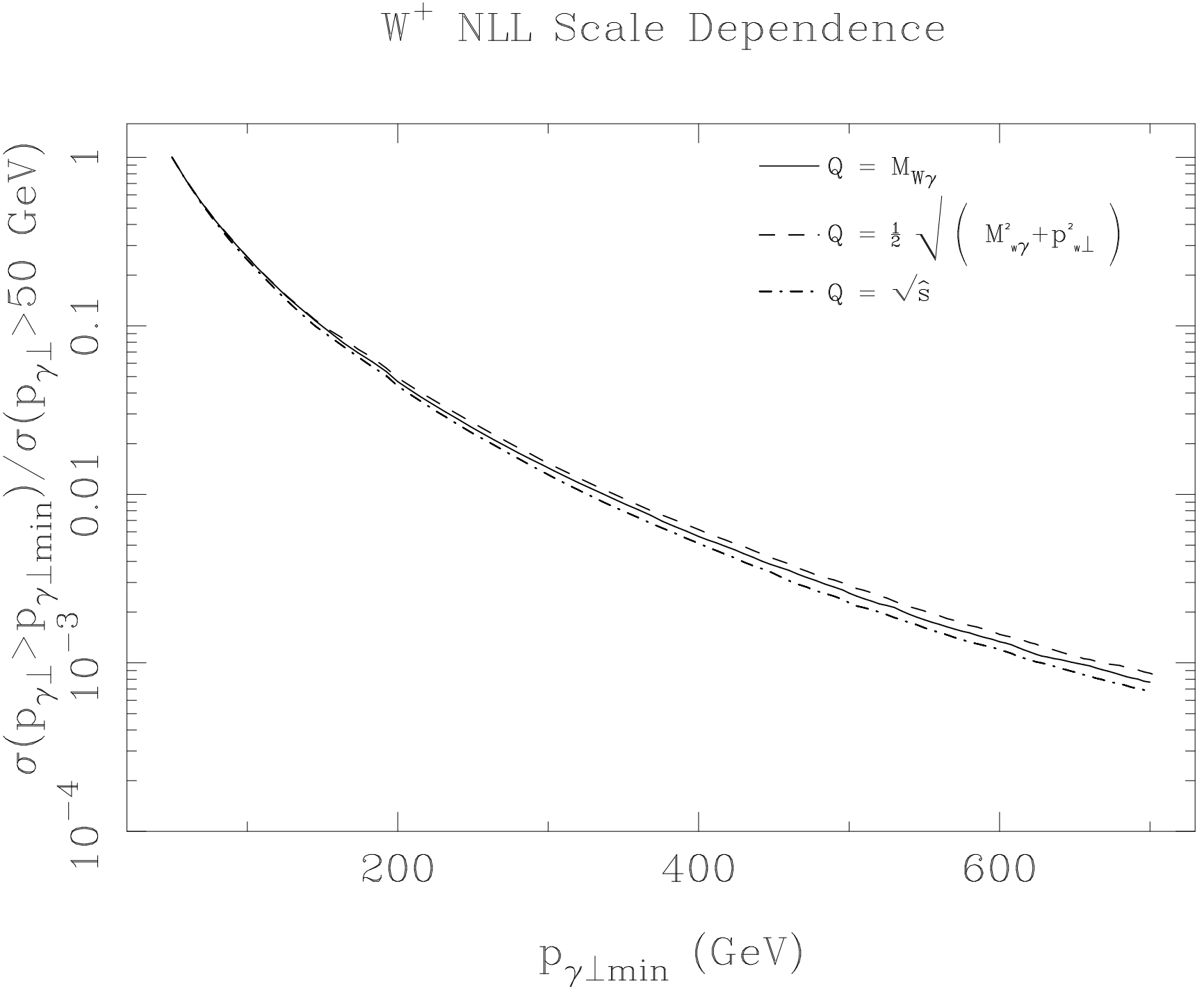
W+ NLL Scale Dependence
Q = M_Wγ
Q = ½ √(M²_wγ + p²_w⊥)
Q = √ŝ
σ(p_γ⊥>p_γ⊥min)/σ(p_γ⊥>50 GeV)
10^-4
10^-3
0.01
0.1
1
200
400
600
p_γ⊥min (GeV)

Figure 6

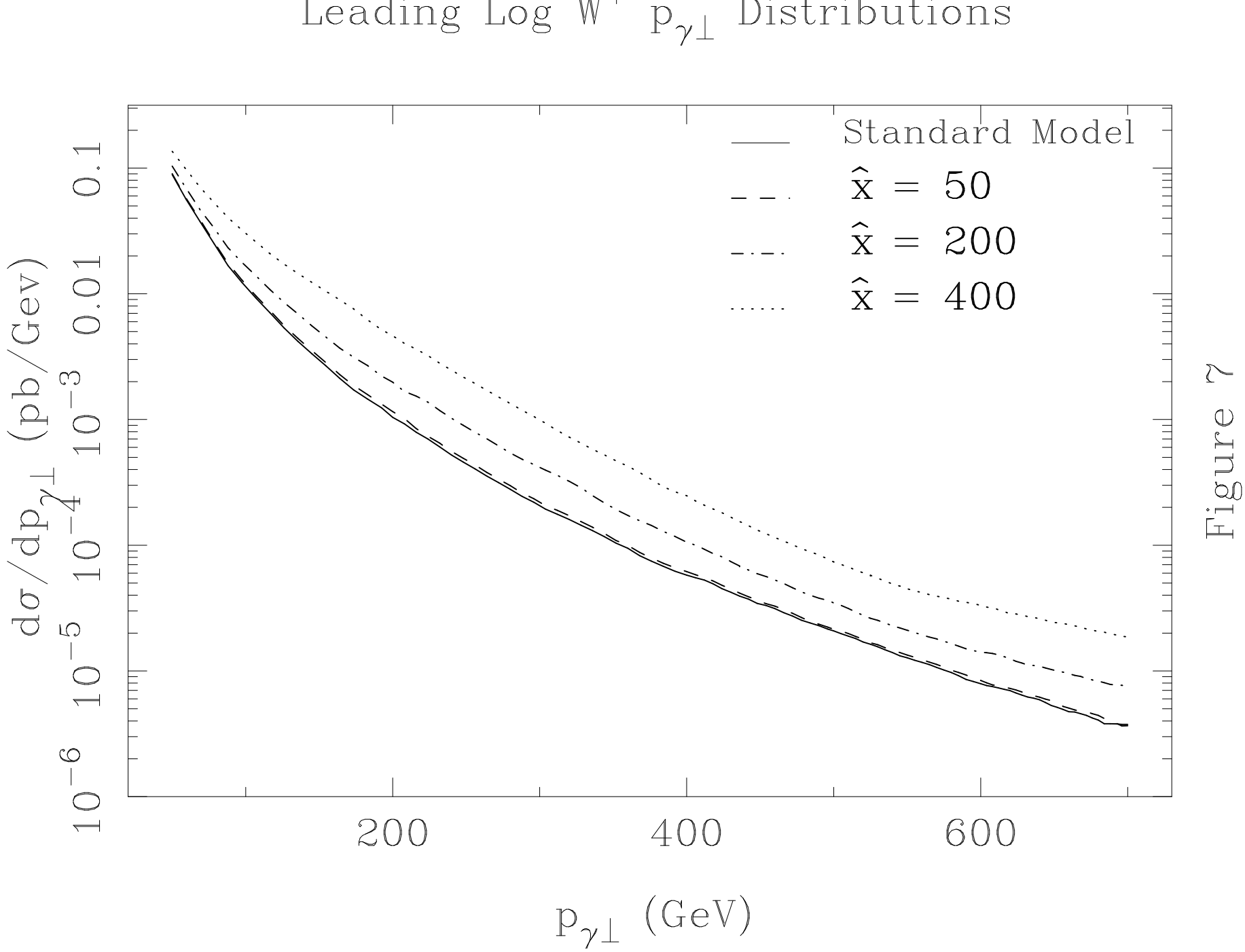
Leading Log W^+ $p_{\gamma\perp}$ Distributions
Standard Model
$\hat{x}$ = 50
$\hat{x}$ = 200
$\hat{x}$ = 400
$d\sigma/dp_{\gamma\perp}$ (pb/Gev)
10^{-6} 10^{-5} 10^{-4} 10^{-3} 0.01 0.1
200 400 600
$p_{\gamma\perp}$ (GeV)

Figure 7

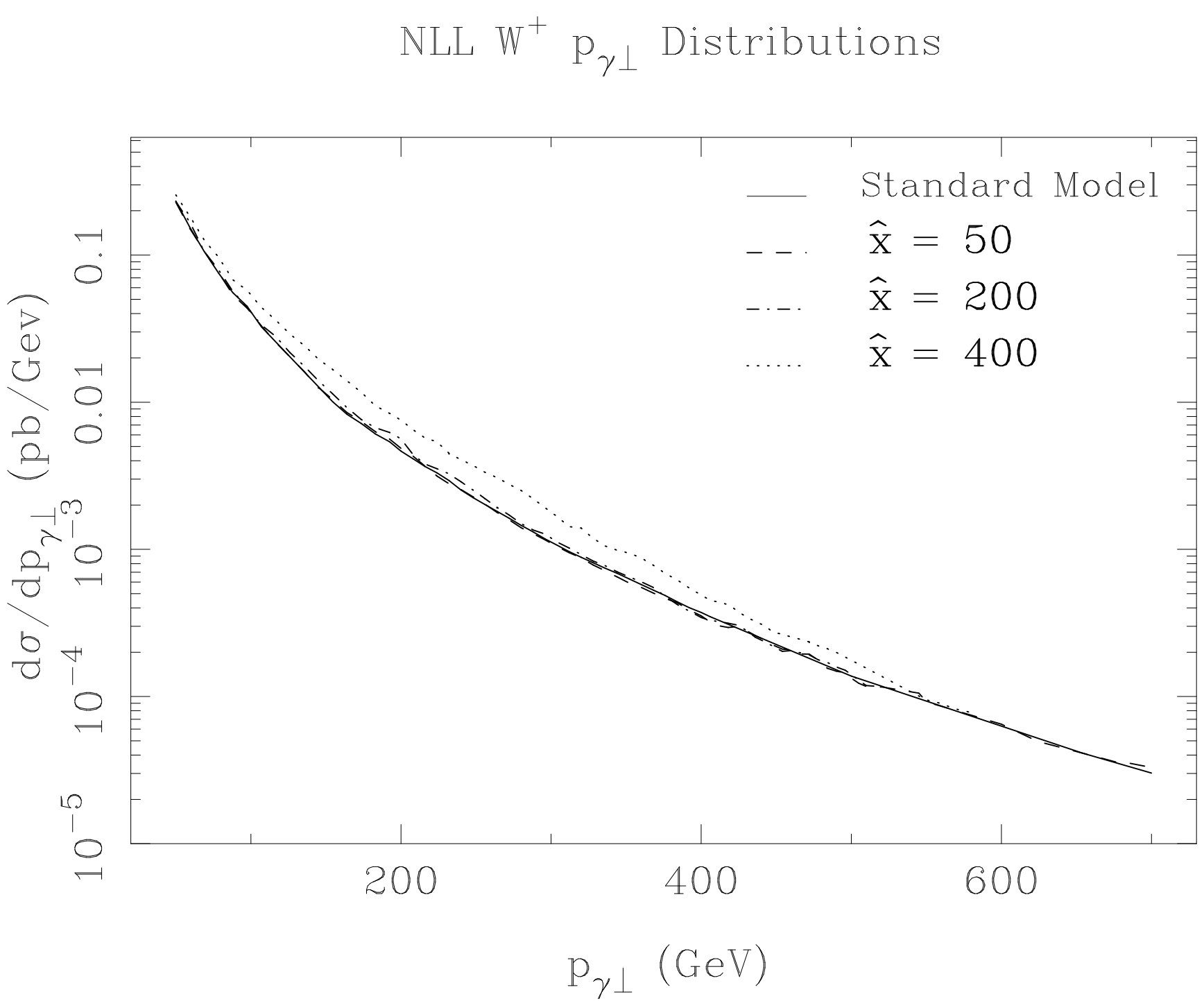
NLL W^+ $p_{\gamma\perp}$ Distributions
Standard Model
$\hat{x}$ = 50
$\hat{x}$ = 200
$\hat{x}$ = 400
$d\sigma/dp_{\gamma\perp}$ (pb/Gev)
10^{-5}
10^{-4}
10^{-3}
0.01
0.1
200
400
600
$p_{\gamma\perp}$ (GeV)

Figure 8